Temperature Dependence of the Free Volume in Fluoroelastomers from Positron Lifetime and PVT Experiments

Günter Dlubek,*,† Asmita Sen Gupta,‡,# Jürgen Pionteck,§ Reinhard Krause-Rehberg,‡ Harald Kaspar,⊥ and K. Helmut Lochhaas⊥

ITA Institute for Innovative Technologies, Köthen, branch office Halle, Wiesenring 4, D-06120 Lieskau (Halle/S.), Germany; Department of Physics, Martin-Luther-University, D-06099 Halle/S., Germany; Institute of Polymer Research Dresden, Hohe Strasse 6, D-01069 Dresden, Germany; Dyneon GmbH & Co. KG, Werk Gendorf, 84504 Burgkirchen, Germany; and Department of Physics, Visva-Bharati, Central University, Santiniketan, West Bengal 731235, India

Received May 12, 2004; Revised Manuscript Received June 21, 2004

ABSTRACT: The microstructure of the free volume and its temperature dependence in fluoroelastomeric copolymers of tetrafluoroethylene (TFE) and perfluoro(methyl vinyl ether) (PMVE), PFE, as well as vinylidene fluoride (VDF) and hexafluoropropylene (HFP), VDF_{78}/HFP_{22}, were studied by pressure−volume−temperature experiments (PVT, $T = 300-485$ K, $P = 0-200$ MPa) and positron annihilation lifetime spectroscopy (PALS, $T = 100-473$ K, $P = 0$ MPa). Employing the Simha−Somcynsky equation of state (S−S eos), the excess free (hole) volume fraction h and the specific free and occupied volumes, $V_f = hV$ and $V_{occ} = (1 - h)V$, were estimated from the specific total volume V. The temperature and pressure variation of these volumes and their expansivity and compressibility will be discussed. The PALS spectra were analyzed using the routine LT9.0 assuming a dispersion in both the positron (τ_2) and ortho-positronium (o-Ps) lifetime (τ_3). From the lifetime parameters the hole size distribution, its mean value $\langle v_h \rangle$ and dispersion σ_h were calculated. From a comparison of $\langle v_h \rangle$ with V and V_f the specific hole number N_h' was estimated. N_h' was determined to be independent of the temperature. Indications were found that o-Ps may prefer larger holes with a weight approximately proportional to the hole volume. Apparent discrepancies between S−S modeling and the conclusions from PALS are discussed. From the comparison of the hole size distribution with the theory of thermal fluctuation a fluctuation volume $\langle V \rangle$ is estimated which decreases above T_g with increasing temperature. Attempts are made to interpret the PALS results in terms of the theory of structural and dynamic heterogeneity of glass-forming liquids.

Introduction

Fluoroelastomers find wide application in petrochemical, automotive, aerospace, and aeronautic industries as sealing material used in extreme temperature ranges.[1,2] Their excellent permeation resistance is an important property to comply with new evaporative emissions regulations. The permeation properties as well as the viscosity, viscoelasticity, the glass transition, volume recovery, and mechanical properties are closely related to the (excess) free volume appearing in amorphous polymers due to their structural, static, or dynamic disorder.[3−5]

This excess free volume appears in form of many irregularly shaped cavities or holes of atomic and molecular dimension (local free volumes).[6,7] Despite a great deal of interest in investigations of free volume in polymers, only limited information about its real structures, the hole dimensions and the size and shape distributions, is available. During the past decade positron annihilation lifetime spectroscopy (PALS) has developed to be the most important method for studying subnanometer size holes in polymers.[8−10] In molecular solids and liquids a fraction of the positrons injected from a radioactive source form positronium,[9] and these can annihilate from the *para* (*p*-Ps, singlet *spin* state) or the *ortho* state (*o*-Ps, triplet *spin* state) with a relative formation probability of 1:3. Three decay components appear in the lifetime spectrum of amorphous polymers, and these are attributed to the annihilation of *p*-Ps, free (not Ps) positrons, and *o*-Ps.

In amorphous polymers Ps is formed in subnanometer size holes of the excess free volume or, if formed elsewhere, is trapped by these holes (Anderson localization) after a diffusion over a short mean path of 1−2 nm. Because of annihilation of o-Ps with an electron other than its bound partner and with opposite spin during a collision with a molecule in the hole wall, the o-Ps lifetime reduces from its value in a vacuum, 142 ns (self-annihilation), to the low nanosecond range (pick-off annihilation).[8−10] The smaller the hole, the higher the frequency of collisions and the shorter the o-Ps life.

PALS itself is able to measure the mean volume of the holes and, with larger limitations, their size distribution,[7,11,12] but not directly the hole density and the hole fraction. However, a correlation of PALS results either directly with the macroscopic volume V or with the (excess) free volume V_f allows one to estimate the hole density.[13−21] V_f may be estimated from the macroscopic volume by employing the Simha−Somcynsky equation of state (S−S eos) theory.[3−5]

To obtain more detailed information on the microstructure of the free volume in glassy and rubbery states of fluoroelastomers and their correlation with the macroscopic volume, we have studied in the current work the temperature dependence of the size of local

† ITA Institute Köthen/Halle.
‡ University of Halle.
§ Institute of Polymer Research Dresden.
⊥ Dyneon GmbH Gendorf.
Central University, Santiniketan, West Bengal.
* To whom correspondence should be addressed: Tel +49-345-5512902; Fax +49-40-3603241463; e-mail gdlubek@aol.com.

10.1021/ma049067n CCC: $27.50
Published on Web 07/31/2004

free volumes (holes) by PALS and of the specific volume, V, by pressure−volume−temperature (PVT) experiments.[22] For this study we have chosen two typical fluoroelastomers: one based on tetrafluoroethylene and the other on vinylidene fluoride.

For analysis of the positron lifetime spectra we used the new routine LT in its latest version 9.0,[23,24] which allows both discrete and log−normal distributed annihilation rates $\lambda = 1/\tau$. From the distribution of the o-Ps annihilation rate, $\lambda_3 = 1/\tau_3$, the mean size and the size distribution of free volume holes can be calculated. These distributions will be correlated with theoretical models describing the thermal volume fluctuation. From the comparison of specific total and free volumes, V and V_f, with the mean hole volume the hole number density is estimated.

Finally, we expect from the application of the routine LT9.0 to obtain new information on the behavior of positrons and Ps in amorphous polymers, on the sensitivity of these probes to the microstructure of the free volume, and on the reliability of different modes of the positron lifetime spectrum analysis.

Experimental Section

Samples. The samples under investigation were two commercial fluoroelastomers made by Dyneon GmbH & Co. KG, Germany (a 3M Co.). One elastomer is a copolymer of tetrafluoroethylene ((−[C_2F_4]−, TFE, 45−85 mol %) and perfluoro(methyl vinyl ether) (−[F_2C−$CF(OCF_3)$]−, PMVE, 15−55 mol %), denoted as Dyneon Perfluoroelastomer PFE (the exact composition is known to the authors). The other elastomer is a copolymer of vinylidene fluoride (−[CF_2CH_2]−, VDF, 78 mol %) and hexafluoropropylene (−[F_2C−$CF(CF_3)$]−, HFP, 22 mol %), denoted as Fluorel FC-2175 (VDF/HFP_{22}). The polymers were pressed at a temperature of 170−200 °C and a pressure of 3−5 MPa for 0.5 h into plates of 2 mm thickness. Subsequently the plates were cooled under laboratory conditions with a rate of approximately 40 K/min. The glass transition temperature T_g was determined using a DSC-7 (Perkin-Elmer), PYRIS software, version 4.01, from the second heat with a rate of 10 K/min (half step method). T_g and further parameters of these elastomers are shown in Table 1.

PVT Experiments. The PVT experiments were carried out by means of a fully automated GNOMIX high-pressure dilatometer.[22] The data were collected in the range from room temperature to 213 °C in steps of ca. 15 K. At every constant temperature the material was pressurized from 10 to 200 MPa, and data were collected in steps of 10 ± 0.1 MPa. The specific volumes for ambient pressure were obtained by extrapolating the values for 10 to 30 MPa in steps of 1 MPa according to the Tait equation using the standard GNOMIX PVT software. The instrument is able to detect changes in specific volume as small as 0.0002 cm^3/g with an absolute accuracy of 0.002 cm^3/g. The densities of the samples at room temperature were determined by means of an Ultrapycnometer 1000 (Quantachrome) with an accuracy of 0.3%.

Positron Lifetime Experiments. The PALS measurements were carried out using a fast−fast coincidence system[8−10] with a time resolution of 232 ps (fwhm of a single Gaussian, ^{22}Na source) and a channel width of 50.0 ps. Two identical samples of 1.5 mm thickness and 8 × 8 mm^2 area were sandwiched around a 1 × 10^6 Bq positron source: ^{22}NaCl, deposited between two 7 μm thick aluminum foils. To prevent sticking of the source to the samples at higher temperatures, each sample was covered with additional foils of 8 μm thick Kapton and 7 μm thick aluminum. The temperature of the samples, placed in a vacuum chamber of a pressure of 10^{-5} Pa, was varied between 100 K and at maximum 473 K, in steps of 15 or 10 K, with an uncertainty of ±1 K. Each lifetime spectrum contained ∼6 × 10^6 coincidence counts which is sufficiently high to be analyzed with LT9.0 in its distribution mode. Source corrections, 9.6% of 386 ps (Kapton and NaCl) and 13.6% of 165 ps (Al foils), and time resolution were determined by measuring a defect-free p-type silicon reference (τ = 219 ps). The final resolution function used in the spectrum analysis was determined as a sum of two Gaussians with fwhms of 222 and 325 ps and weights of 80.9% and 19.1%; the second Gaussian is shifted by −0.26 channels with respect to the first one.

Table 1. Sample Characterization and Volume Parameters Estimated from the PVT Data (Data at 300 K, If Not Specified)

denotation	uncertainty	PFE	VDF/HFP_{22}
trade name		Dyneon PFE	Fluorel FC-2175
components		TFE/PMVE	VDF/HFP
M_{rep} (g/mol)		100.02/166.02	64.03/150.02
molar composition		45−85:55−15[a]	78:22
M_w (kg/mol)	±10%	100	85
T_g (DSC, K)	±3	271	255
T_0' (K)	±10	180	200
V (cm^3/g)	±0.002	0.4811	0.5554
V_W (cm^3/g)		0.2994	0.3550
V_{occ} (cm^3/g)	±0.003	0.431	0.513
V_f (cm^3/g)	±0.003	0.051	0.043
h	±0.003	0.105	0.078
$h(T_g)$	±0.004	0.084	0.050
α (10^{-4} K^{-1})	±0.05	8.67	6.83
α_{occ} (10^{-4} K^{-1})	±0.05	0.38	0.31
α_f (10^{-3} K^{-1})	±0.1	7.24	9.05
κ (10^{-4} MPa^{-1})	±0.05	7.87	5.70
κ_{occ} (10^{-4} MPa^{-1})	±0.1	2.5	2.4
κ_f (10^{-3} MPa^{-1})	±0.2	5.3	4.3
T^* (K)	±50	8038	9281
V^* (cm^3/g)	±0.003	0.4501	0.5374
P^* (MPa)	±10	749	850
$\langle M_{rep} \rangle$ (g/mol)		123.1	82.95
M_0 (g/mol)	±0.3	63.2	53.9
ω (Å^3)	± 0.5	45.2	45.9
H_h (kJ/mol)	0.04	5.60	6.24

[a] Exact composition is known to the authors.

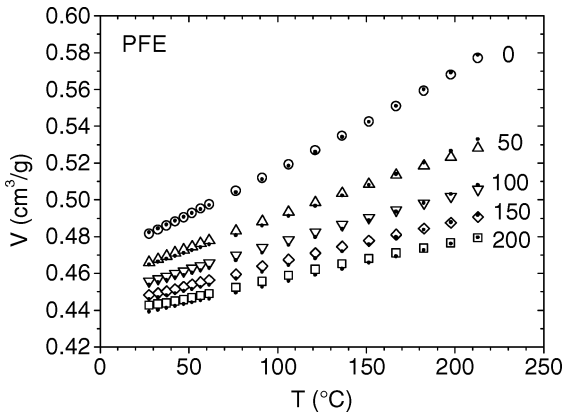

Figure 1. Specific volume V of PFE as a function of temperature T and as selection of isobars (P in MPa). Open symbols: experimental data; dots: S−S eos fits (eq 2).

Results and Discussion

Specific Volume and S−S eos Analysis of PVT Data. Figures 1 and 2 show the temperature dependence of the specific volume V of PFE and VDF/HFP for selected pressures P. We analyzed these data employing the S−S eos theory. This theory describes the structure of a liquid by a cell or lattice model (coordination number z = 12) which allows an occupied lattice-site fraction $y = y(V, T)$ of less than one. It is assumed that N molecules, consisting of n chemical repeat units, n-mers, with molecular weight M_{rep}, are divided into s equivalent segments, s-mers, with molecular weight M_0, $sM_0 = nM_{rep}$. The number sN of s-mer molecules occupy

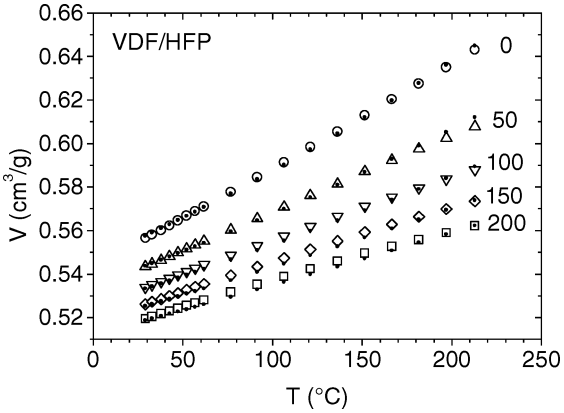

Figure 2. As in Figure 1, but VDF/HFP_{22}.

randomly the fraction $y = sN/(sN + N_h^{SS})$ of the total available sites, $(sN + N_h^{SS})$, where N_h^{SS} is number of unoccupied lattice sites or holes of the S−S theory. The fraction of unoccupied lattice sites (holes), which is denoted in this theory by h, is given by $h(V,T) = 1 - y$.

The Simha−Somcynsky equation of state[3−5] follows from the pressure equation $P = -(\partial F/\partial V)_T$, where $F = F(V,T,y)$ is the configurational (Helmholtz) free energy F of the liquid

$$\frac{\tilde{P}\tilde{V}}{\tilde{T}} = [1 - y(2^{1/2}y\tilde{V})^{-1/3}]^{-1} + \frac{y}{\tilde{T}}[2.002(y\tilde{V})^{-4} - 2.409(y\tilde{V})^{-2}] \quad (1)$$

$\tilde{P}$, $\tilde{V}$, and $\tilde{T}$ are reduced variables, $\tilde{P} = P/P^*$, $\tilde{V} = V/V^*$, and $\tilde{T} = T/T^*$, where P^*, V^*, and T^* are characteristic scaling parameters. The occupied volume fraction y is coupled with $\tilde{T}$ and $\tilde{V}$ in a second equation derived from the minimization condition $(\partial F/\partial y)_{V,T} = 0$ and assuming for polymers $s \rightarrow \infty$ and a flexibility ratio of $s/3c = 1$.[3−5] The molecular weight of a s-mer, M_0, is related to the scaling parameters via $M_0 = RT^*/3P^*V^*$, where R is the gas constant. It was shown that both equations may be replaced in the temperature and pressure ranges $\tilde{T} = 0.016-0.071$ and $\tilde{P} = 0-0.35$ by the universal interpolation expression

$$\ln \tilde{V}(P,T) = a_0 + a_1\tilde{T}^{3/2} + \tilde{P}[a_2 + (a_3 + a_4\tilde{P} + a_5\tilde{P}^2)\tilde{T}^2] \quad (2)$$

(Utracki and Simha,[5] $a_0 = -0.10346$, $a_1 = 23.854$, $a_2 = -0.1320$, $a_3 = -33.7$, $a_4 = 1032.5$, $a_5 = -1329.9$). We estimated the scaling parameters P^*, V^*, and T^* from nonlinear least-squares fits of eq 2 to the volume data. To evaluate the PVT data in comparison with the PALS results, we are most interested in good fits of the zero pressure isobars. Therefore, we have used the traditional consecutive evaluation procedure.[27] First T^* and V^* were determined from nonlinear least-squares fits of eq 2 to the volume data for $P = 0$ MPa (ambient pressure) and $T = 27-213$ °C. Typical coefficients of determination of $C_d = 0.9998$, correlation coefficients squared of $r^2 = 0.9997$, and standard deviations of $s = 0.0005$ were obtained. The maximum deviation of the fitted curve from the experimental data amounts to 0.0025 cm³/g; the mean deviation is less than half as large. In a second fit including the data from the PVT field in the range 27−213 °C and 0−200 MPa and fixing

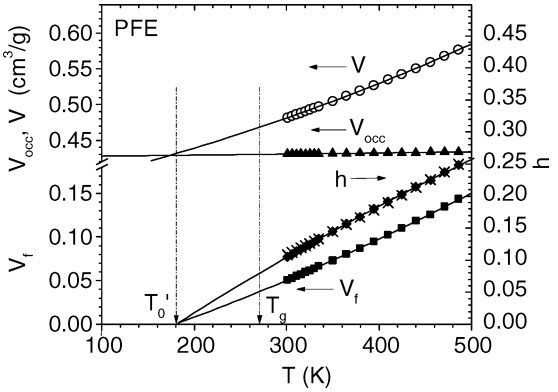

Figure 3. Specific (total) volume V (open circles), the hole fraction h, and the specific occupied and free volumes $V_{occ} = (1 - h)V$ and $V_f = hV$ for PFE at ambient pressure. The hole fraction h calculated from eq 1 is shown as diamonds while the crosses show the results of the algebraic eq 3. The solid lines are linear (V_{occ}) or quadratic fits (V, V_f, h) and extrapolations. T_g is from DSC, and T_0' indicates the temperature where the extrapolated excess free volume disappears.

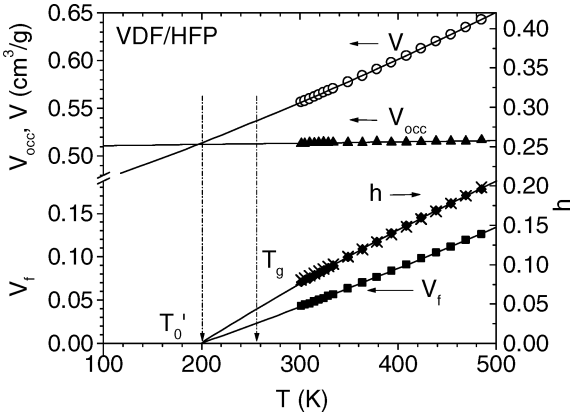

Figure 4. As in Figure 3, but VDF/HFP_{22}.

T^* and V^* to the former values, the scaling pressure P^* was found.

The results of the fits are displayed in Table 1. The derived parameters have to be considered as average quantities describing the PVT behavior of the copolymers. As Figures 1 and 2 show, the overall description of the experiments in the selected temperature and pressure range is good. The scaling volumes, V^*, have a ratio to the van der Waals volume, V_W, of $V^*/V_W = 1.50$ (PFE) and 1.49 (VDF/HFP_{22}). The van der Waals volumes were calculated from the Bondi group contribution method[25] using the data collected by van Krevelen.[26] The ratios for our fluorine copolymers are close to that found by other groups for a larger variety of polymers, ∼1.45[27] and 1.57−1.60.[16]

Using the scaling parameters, we have calculated the fractions of occupied sites, y, and hole sites, $h = 1 - y$, from a numerical solution of eq 1. Figures 3 and 4 show, together with the specific volume V, the results of our analysis in the temperature range between 300 and 486 K for ambient pressure displayed as the hole fraction h (the fractional free volume), the specific free volume $V_f = hV$, and the specific occupied volume $V_{occ} = yV$. As in the S−S eos, we assume that the partial volumes V_{occ} and V_f behave additively and are exposed to the same temperature T and hydrostatic pressure P as applied externally to the sample, $V(T,P) = V_{occ}(T,P) + V_f(T,P)$. Under these assumptions, their expansivities and compressibilities also behave additively.

The thermal expansions of V, h, and V_f are slightly parabolic, while V_{occ} changes linearly. From the linear or parabolic fits to volume data we calculated the isobaric coefficients of thermal expansion, $\alpha_i = (1/V_i)(dV_i/dT)_P$ ($i = occ, f$), of the occupied and free volume. The isothermal compressibilities, $\kappa_i = -(1/V_i)(dV_i/dP)_T$ ($P \rightarrow 0$), were estimated from fits of a polynomial of fourth degree to the volume data. The parameters of the total volume, α and κ, can be calculated directly from the derivatives of eq 2. The results, valid for room temperature (300 K) and ambient pressure, are shown in Table 1.

The fractional free volume h increases from 0.084 (extrapolated) to 0.25 for PFE and from 0.051 (extrapolated) to 0.20 for VDF_{78}/HFP_{22} when the temperature rises from T_g(DSC) to 486 K (Figures 3 and 4). The numerical data can be compared with the universal algebraic expression

$$h(P,T) = a_0 + a_1\tilde{T} + a_2\tilde{T}^2 \qquad (3)$$

derived for $P = 0$ in the paper of Utracki and Simha[5] ($a_0 = -0.9211$, $a_1 = 4.892$, $a_2 = 12.56$). As shown in Figures 3 and 4, eq 3 (crosses) fits well the numerical data.

The data in Table 1 show that the coefficient of the thermal expansion of the free volume, α_f, is 1 order of magnitude larger than that of the total volume, α, while the occupied volume shows almost no thermal expansion, $\alpha_{occ} \approx 0.3 \times 10^{-4}$ K^{-1}. The compressibilities exhibit another behavior. Between room temperature and 200 °C, $\kappa(P = 0)$ increases for PFE from 7.9×10^{-4} to 16.8×10^{-4} MPa^{-1} (not shown). The compressibility of the free volume changes only slightly and is 1 order of magnitude larger than that of the total volume, $\kappa_f = (5.3-5.8) \times 10^{-3}$ MPa^{-1}. The κ_{occ} values are almost constant, $\kappa_{occ} \approx 2.5 \times 10^{-4}$ MPa^{-1}. Our results show that the total volume varies with the temperature and pressure mainly because of the variation in the free volume fraction. The κ_{occ} values estimated here are larger than the typical compressibility of polymer crystals. From the data published by Jain and Simha,[28] zero-pressure compressibilities of 1.5×10^{-4} MPa^{-1} (20 °C) and 1.6×10^{-4} MPa^{-1} (66 °C) can be estimated for polyethylene crystals. The analysis of the VDF/HFP_{22} behavior leads to corresponding results as for of PFE except slightly smaller values for α and κ (Table 1).

Our results show clearly that the occupied volume, $V_{occ} = yV$, calculated from the S−S eos shows a very weak thermal expansion but is compressible (all at $T > T_g$). The reason for this is that V_{occ} contains an empty space, frequently termed as interstitial free volume V_{fi}, which can be calculated as difference between the occupied and the van der Waals volume, $V_{fi} = V_{occ} - V_W$. Its expansivity and compressibility differ from that of the "excess" free volume V_f. V_f depends on the route in the $T-P$ plane on which a given total volume V is reached. From this follows that the observation of different relaxation properties for the same total volume or density[4,29] does not necessarily contradict the free volume theory as it has been sometimes concluded.[29] The total volume is not the controlling parameter of the mobility, but the excess free volume (associated with the special type of mobility) is. In this context we notice that the (parabolic) extrapolation of h and V_f down to zero values delivers a characteristic temperature which we have denoted as T_0' (Figures 3 and 4). In a naive picture T_0' should correspond to the temperature where the mobility in a polymer disappears.[19,20] This temperature is known as the Vogel temperature T_0.

$V_{occ}(T)$ mirrors directly the variation of the cell volume $\omega = yV/sN$. It can be estimated from the equations $\omega = (M_0/M_{rep})V_{rep}(T) = M_0V_{occ}(T)/N_A$ and $M_0 = RT^*/3P^*V^*$, where N_A is Avogadro's number. Our scaling parameters deliver a molecular mass of mers occupying the lattice cells of $M_0 = 63.2$ g/mol (PFE) and 53.9 g/mol (VDF/HFP_{22}). These values correspond to ratios of $M_0/\langle M_{rep}\rangle = 0.51$ (PFE) and 0.65 (VDF/HFP_{22}), where $\langle M_{rep}\rangle$ is the average molecular mass of the effective repeating unit calculated from the composition weighted average of the molecular masses of the constituents of both copolymers (Table 1). The values of $M_0/\langle M_{rep}\rangle$ vary for different type of polymers between 0.25 and 1.25.[30] From our values for $M_0/\langle M_{rep}\rangle$ cell volumes at 300 K of $\omega = (M_0/\langle M_{rep}\rangle)\langle V_{rep}\rangle = M_0V_{occ}/N_A = 45.2$ Å^3 (PFE) and 45.9 Å^3 (VDF/HFP_{22}) follow (N_A = Avogadro's number). $\langle V_{rep}\rangle$ is the average volume of the effective repeating unit being 88.1 Å^3 for PFE and 70.6 Å^3 for VDF/HFP_{22}.[26]

The total increase of the specific free volume V_f comes mainly from the creation of new empty cells. To study the real variation in the number of created holes, N_h^{SS}, we have to consider the hole number related to the number of occupied lattice sites, sN. Its variation per 1 K, $d(N_h^{SS}/sN)/dT = d(V_f/V_{occ})/dT = d(h/y)/dT$, amounts to 11.3×10^{-4} K^{-1} for PFE and to 8.8×10^{-4} K^{-1} for VDF/HFP_{22}. Both values are larger than that found for PS, 6.7×10^{-4} K^{-1}.[20]

When we tentatively consider the holes as point defects in a lattice (quasi-point defect model[31]), their equilibrium concentration per lattice site may be calculated from

$$h = N_h^{SS}/(sN + N_h^{SS}) = \exp(S_h/k_B)\exp(-H_h/k_BT) \qquad (4)$$

with

$$H_h = -k_B\,\partial[\ln h(T,P)]/\partial[1/T]|_P$$

where H_h and S_h are the enthalpy and the entropy of the hole formation and k_B is the Boltzmann constant. Equation 4 derives from minimizing the Gibbs free energy with respect to the hole number assuming no interaction between holes. Since N_h^{SS} cannot be neglected in comparison with sN, we have to consider here the quantity $h = h/(h + y)$ and not, as usually done,[20] the point defect concentration $C_h = N_h^{SS}/sN = h/y$.

Arrhenius plots of log h vs $1/T$ show straight lines (Figure 5) with a typical variance of 0.005 and r^2 value of 0.9998. From the fits a molar activation enthalpy for the hole formation in PFE of $H_h = 5.60$ kJ/mol and in VDF/HFP_{22} of $H_h = 6.24$ kJ/mol and S_h/R equal to 0.99 and 0.93, all at ambient pressure, can be estimated. The fit parameters correspond to $H_h = (2.5-2.9)RT_g$, which is close to $H_h \approx 3RT_g$ estimated by Perez[31] from calorimetric data, while our S_h/R values correspond to these estimates, $S_h/R \approx 1.8-2$, when taking into account that for comparison $\ln(M_{rep}/M_0) \approx \ln 2$ must be added to our value.

If one imagines the hole creation as formation of a Schottky defect, i.e., an s-mer migrates to a typical surface site leaving an unoccupied lattice site in the interior of the sample, then the hole formation enthalpy H_h should approximately correspond to half of the cohesive energy of the s-mers. From the algebraic expression for the cohesive energy density CED =

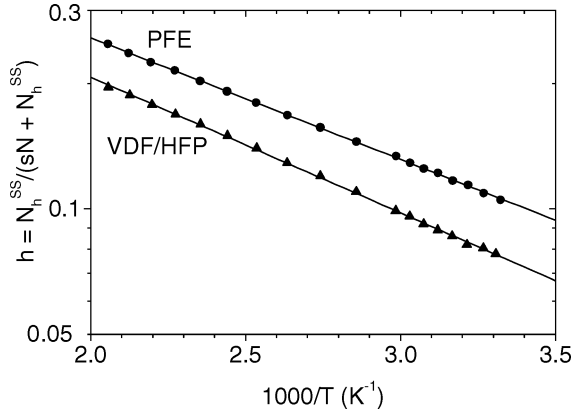

Figure 5. Arrhenius plot of the relative number of empty lattice sites (holes), $h = N_h^{SS}/(sN + N_h^{SS})$, for PFE (circles) and VDF/HFP$_{22}$ (triangles, straight lines: linear fits). The temperature range is $T = 300-485$ K.

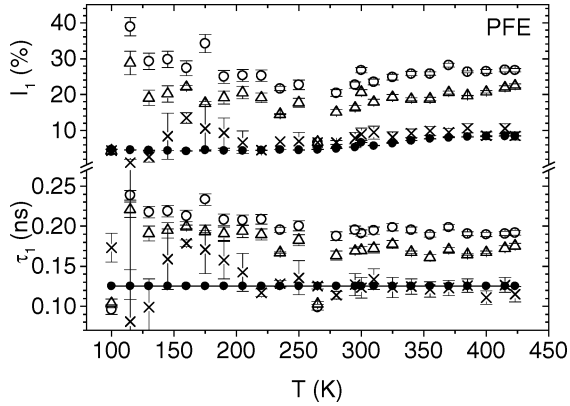

Figure 6. Lifetime τ_1 and intensity I_1 of the first component (p-Ps) of the lifetime spectrum of PFE as a function of temperature, T. The spectra were decomposed into three components under different assumptions: (i) only discrete components (open circles), (ii) allowing a dispersion in τ_3 (open up-triangles), (iii) allowing a dispersion in τ_2 and τ_3 (crosses, all these analysis without constraining any parameter), and (iv) allowing a dispersion in τ_2 and τ_3 but constraining $\tau_1 =$ 125 ps and $I_1/I_3 = 1/3$ (filled circles).

$C\tilde{E}D(\tilde{V}, \tilde{T}) \times P^*$ given by Utracki and Simha (eqs 13 and 17 in ref 5), we have estimated cohesive energy of s-mers of $E_c = CED(M_0/\rho)$ ($\rho = 1/V$) of 12.93 kJ/mol (300 K) to 11.0 kJ/mol (486 K) for PFE and14.0 kJ/mol (300 K) to 11.8 kJ/mol (486 K) for VDF/HFP$_{22}$. These energies are close to double the values found for H_h (Table 1). The decrease of E_c with increasing temperature is mirrored in a slight curvature of the Arrhenius plots and a slight variation of $H_h(T)$ with the temperature. From our data we found the ratio $K(\tilde{T}) = V_{occ}/V^* = 0.957$ (300 K) − 0.963 (473 K) for PFE. In the literature $h(T, P = 0)$ is frequently calculated from the simple approximation $h = 1 - K/\tilde{V}$, assuming a constant $K = 0.95$.[3,5] The value of $V_{occ}(300\ K) = 0.431$ cm^3/g corresponds well to the specific crystalline volume of PTFE (form I) of $V_c = 0.442$ cm^3/g.[32] The corresponding values for VDF/HFP$_{22}$ are $K(T/T^*) = V_{occ}/V^* = 0.955$ (300 K) − 0.962 (473 K) and $V_{occ}(300\ K) = 0.513$ cm^3/g. The latter value corresponds to the crystalline volume of PVDF, $V_c = 0.500$ cm^3/g.[26]

Positron Lifetime Spectra and Their Analysis. Conventionally, the lifetime spectra of amorphous polymers are decomposed into three discrete exponentials,[8−10] $s(t) = \sum(I_i/\tau_i) \exp(-t/\tau_i)$, $\sum I_i = 1$, $i = 1, 2, 3$, where the components are attributed to annihilation of p-Ps, $\tau_1 =$ 125−200 ps, free (e^+, not Ps) positrons ($\tau_2 = 300-500$ ps), and o-Ps, $\tau_3 = 1-10$ ns. Since o-Ps annihilates from holes of the free volume, which have a size and shape distribution, the o-Ps lifetime,[11,12] and probably also the e^+ lifetime,[33] will show a distribution. As mentioned, LT in its distribution mode assumes that for some, or all, of the annihilation channels the annihilation rates λ, $\lambda = 1/\tau$, follow a log−normal function.[23,24] The nonlinear least-squares fit of these functions, convoluted with the resolution function, to the spectrum provides the mean lifetime τ_i and the corresponding intensity I_i of the annihilation channel i as well as the width of the corresponding distribution (dispersion or standard deviation σ_i of the lifetime τ_i).

The assumption in LT9.0 of normal distributed annihilation rates λ for each annihilation channel comes from the many years experience with the routine CONTIN,[34] a Laplace inversion technique, which delivers for amorphous polymers usually three Gaussian-like peaks in the log λ space. Similar distributions are analyzed with MELT,[35] a maximum-entropy technique. The advantage of LT9.0 is that the fixing of the functional shape of the distribution reduces distinctly the degree of freedom in the fits, avoids artifacts,[36] and reduces remarkably the scatter in the width of the analyzed distributions. The analysis of our lifetime spectra with CONTIN and MELT delivered similar annihilation parameters to LT9.0 with somewhat smaller dispersion in the lifetimes.[36] We will consider in this paper therefore only the results obtained from LT9.0.

First, we will discuss different modes of analyzing the lifetime spectra and the consequences for the obtained fitting parameters. This point is important since there is the danger of producing incorrect annihilation parameters in the spectrum analysis by making simplifying but incorrect assumptions. It is standard to analyze the lifetime spectra assuming discrete lifetime components, usually by employing the well-accepted routine POSITRONFIT of the package PATFIT[37] or similar routines. For amorphous materials, discrete lifetime components may, however, be a too crude approximation. Since the o-Ps lifetimes in fluoroelastomers are rather large, in particular in PFE, we hope to be able correctly to resolve the components, taking into account the lifetime dispersion in those annihilation channels where they may be important. We will compare the annihilation parameters obtained from a three-component analysis assuming (i) only discrete components, (ii) allowing a dispersion in τ_3, (iii) allowing a dispersion in τ_2 and τ_3 (all these analysis without constraining any lifetime parameter), and (iv) allowing a dispersion in τ_2 and τ_3 and constraining τ_1 and I_1/I_3 to the theoretically expected values.

Figures 6−9 show the annihilation parameters for PFE, presented as an example, analyzed under these different assumptions. In Figure 6, the lifetime and intensity of the first component, τ_1 and I_1, are displayed. This component is due to p-Ps, which decays mainly via self-annihilation. Because of its short life, the annihilation of p-Ps is almost unaffected by material properties, but this component mirrors most sensitively the correctness of the spectrum decomposition. The p-Ps lifetime in matter is given by $\tau_1 = \tau_{p-Ps} = (\eta/\tau^0_{p-Ps} + 1/\tau_{po})^{-1} \approx \tau^0_{p-Ps}$, where $\tau^0_{p-Ps} = 125$ ps denotes the lifetime of p-Ps in a vacuum (self-annihilation) and $\tau_{po} = \tau_3 \gg \tau^0_{p-Ps}$ is the lifetime due to pick-off annihilation. η is the so-called contact density or relaxation parameter

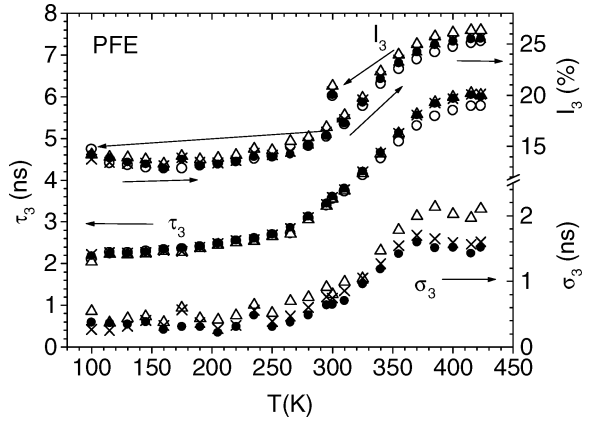

Figure 7. As in Figure 6, but the lifetime, τ_3, its dispersion, σ_3, and the intensity, I_3, of the third (o-Ps) component of the lifetime spectrum. The arrows at the I_3 curve indicate the thermal history. I_3 (but not the lifetime) shows a hysteresis when being annealed at temperatures above 370 K which can be observed for the data at 300 K. For clarity the error bars were omitted.

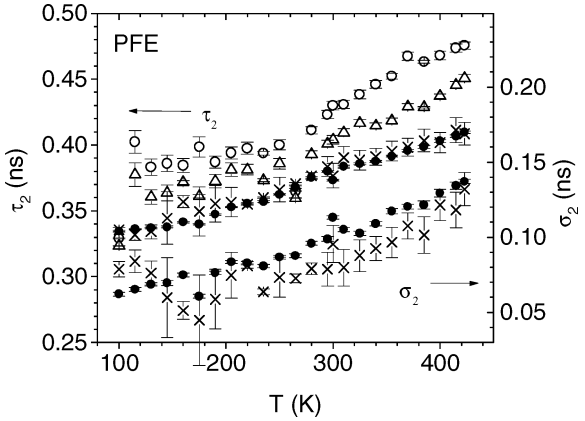

Figure 8. As in Figure 6, but the lifetime τ_2 and its dispersion σ_2 of the second (e^+) component of the lifetime spectrum.

which describes the relaxation of Ps in matter compared with the state in a vacuum.[9] The diameter of the Ps probe is $0.106\eta^{-1/3}$ nm. Estimates from magnetic quenching experiments suggest that in polymers η may have values between 0.5 and 1; for PTFE $\eta = 1$ has been estimated.[38] From this considerations we expect a lifetime of $\tau_1 \approx 125$ ps without remarkable dispersion around this value and an intensity corresponding to the theoretical ratio of p-Ps to o-Ps formation, $I_1/I_3 = 1/3$. Moreover, we assume, as is usual, that p-Ps and o-Ps annihilate only via self-annihilation and pick-off, respectively, and that there is no chemical or magnetic quenching.

As can be observed in Figure 6, the values for τ_1 and I_1 from the discrete term analysis are too large compared with the theoretical expectation. (We remark that LT in its discrete mode delivers the same lifetime parameters as the traditional routine POSITRONFIT.[37]) This effect is well-known and sometimes attributed to the finite resolution of the positron experiment. Some of us have shown, however, that this effect does not appear for simulated discrete spectra but may be explained as an artifact of the discrete-term analysis of spectra having a distribution in τ_3, and, more importantly, in τ_2.[33] When τ_3 is allowed to be distributed, the effect is only slightly reduced. When dispersion in both τ_2 and τ_3 is allowed, τ_1 and I_1 values are found, which correspond very well with the theoretical expectations. Fits with τ_1 and I_1/I_3 constrained reduce the statistical scattering of I_1 and all other annihilation parameters and provide the same parameters as the analysis (iii). The reduced chi-squares of the fits, χ^2/df, varied for the last two modes of analysis between 0.97 (100 K) and 1.12 (473 K); the fit to the spectra was started 8 channels (0.4 ns) left of the maximum. χ^2/df reduces further when less channels left of the maximum are involved, but then the time zero and due to this, the first component may be incorrectly determined. χ^2/df is clearly larger in the second (1.2−1.4) and first mode (1.3−1.6) of analysis.

Figure 7 shows the (mean) lifetime, τ_3, its dispersion, σ_3 (the standard deviation of its distribution), and the intensity, I_3, of the o-Ps annihilation. τ_3 changes from 2.2 ns at 100 K to 6.0 ns at 423 K and shows a rapid increase in its slope around 250 K and a leveling off at a temperature of $T_k = 380$ K (o-Ps-"knee" temperature). σ_3 shows a similar variation as τ_3 but between 0.4 and 1.5−2 ns, and I_3 varies between 14% and 26%. As can be observed, the annihilation parameters obtained from the various analyses differ slightly. At higher temperatures (lifetimes) the discrete term analysis leads to a slight but nonnegligible underestimation of τ_3 and I_3, while when allowing only τ_3 to be distributed, I_3 and the dispersion, σ_3, are overestimated. The effect on τ_3 is weak. Including the distribution of τ_2 and τ_3 into the analysis, almost the same parameters are obtained as with the constrained analysis technique (iv).

The behavior of the second lifetime which mirrors the e^+ (not Ps) annihilation is also of physical interest. As Figure 8 shows, τ_2 obtained from discrete term fits exhibits a behavior very similar to τ_3. That behavior has been observed in past and interpreted as evidence for the positrons being localized at holes of the (excess) free volume like o-Ps atoms, and their lifetime mirrors the variation in the hole size with the temperature.[39] Our results show, however, that the change in the thermal expansivity of τ_2 at T_g is reduced when allowing a dispersion in τ_3. When allowing dispersion in both τ_2 and τ_3, then τ_2 shows only a very weak response to the glass transition and the "knee" at 380 K seems to disappear. Obviously, the similarity of the behavior of τ_2 and τ_3 is largely an artifact of fitting the polymer spectra by discrete terms. This results in a coupling of τ_2 to τ_3 and the overestimation of τ_2. The final analysis (iv) shows an almost linear variation of τ_2 from 0.34 to 0.41 ns and of σ_2 from 0.06 to 0.14 ns when the temperature changes from 100 to 423 K with a slight change in the slopes of both values at 250 K. From this behavior we conclude that positrons (e^+) might annihilate in both regions of the total free volume: the interstitial free volume and the excess free volume. The interstitial free volume covers a fraction of approximately $(1.45-1)V_W = 0.45V_W$, while the excess free volume has a fraction of $(1.60-1.45)V_W = 0.15V_W$.[26] The interstitial free volume may expand like in PTFE crystals.[40] This behavior combined with the changes in the excess free volume at the glass transition may explain the observed expansion of τ_2. The dispersion in τ_2 may mirror the effect of molecular vibrations on the interstitial free volume and local fluctuations on the excess free volume.

We remark that an analysis of the lifetime spectra using the constrainment $\tau_1 = 0.125$ ns and $I_1/I_3 = 1/3$, but not allowing a dispersion in τ_2, gives too large values of σ_3 and $\chi^2/df \approx 2.5$. An artificial increase or decrease

in the width of the resolution function by 0.010 ns results in larger or smaller values for σ_2 and in too small or too larger values for σ_3 and in an increase of χ^2/df to $\approx$3. We can discount the possibility that the observed dispersion in the lifetime τ_2 is due to a possible mixing of the e^+ lifetimes with the lower wing of the o-Ps lifetime distribution, since a distribution in the e^+ lifetimes has been observed by some of us previously in the polyimide Kapton, which shows no Ps formation.[33]

The spectrum analysis for VDF/HFP_{22} delivers similar results as found for PFE. Figure 9 shows the o-Ps lifetime, τ_3 (mode iv of analysis), and its dispersion, σ_3, for VDF/HFP_{22} in comparison with PFE. The o-Ps lifetime τ_3 changes from 1.65 to 4.28 ns when the temperatures increases from 100 to 373 K while σ_3 varies from 0.4 ns 1.2 ns. Both values, τ_3 and σ_3, of VDF/HFP_{22} are distinctly smaller than those of PFE, except the similar values of σ_3 below T_g. The o-Ps intensity I_3 is distinctly smaller than for PFE and changes almost linearly from 7% to 14%. τ_2 increases from 0.35 to 0.42 ns and σ_2 from 0.06 to 0.09 ns.

Hole Size Distribution and the Mean Hole Size. In the following we focus our discussion on the mean hole size and the hole size distribution calculated from the o-Ps lifetime distribution (LT9.0 in mode iv). The o-Ps intensity I_3 does not have a clear relation to the free volume,[17,41] but instead mirrors the Ps formation probability P, $I_3 = 3P/4$.[9] This value is affected by many different parameters; therefore, we will not attempt to interpret this parameter in terms of the free volume. We remark, however, that we observed a hysteresis in I_3 when comparing heating and cooling runs of PFE (see Figure 7). We found that isochronal annealing increases the o-Ps yield I_3 in the temperature range between 320 and 370 K by 2% but does not change the lifetime parameters τ_i and σ_i. This behavior may be attributed to the out-diffusion of small molecules remaining from the polymer synthesis such as hydrogen fluoride or residual water which are inhibitors for the Ps formation. Because of this effect, we annealed a second, fresh sample in a vacuum for 4 h at 120 °C and measured it between room temperature and 473 K during heating (10 K steps) and cooling (15 K steps). The results of this second cycle are included in the following figures and discussion. For VDF/HFP_{22} we did not observe a hysteresis in any lifetime parameter.

The mean hole volume may be calculated in several different ways. First, we used the usual way to calculate the mean radius $r_h(\tau_3)$ of the holes (assumed spherical) from the mean o-Ps pick-off annihilation rate $\lambda_{po} = \lambda_3 = 1/\tau_3$ using the equation

$$\lambda_{po} = 1/\tau_{po} = 2\ \mathrm{ns}^{-1}\{1 - [r_h/(r_h + \delta r)] + (1/2\pi)[\sin(2\pi/(r_h + \delta r))]\} \quad (5)$$

This equation comes from a semiempirical model[42] which assumes that o-Ps is localized in an infinitely high potential well with the radius $r_h + \delta r$, where r_h is the hole radius and the empirically determined $\delta r = 1.66$ Å[8,43] describes the penetration of the Ps wave function into the hole walls. The relation $\lambda_{po} = 1/\tau_{po} = 1/\tau_3$ is based on the assumption that spin conversion and chemical quenching of Ps[9] are negligible. The mean hole volume then follows from $v_h(\tau_3) = (4/3)\pi r_h^3(\tau_3)$.

As a second way we have calculated the mean hole volume as mass center of the hole volume distribution. As already mentioned, the routine LT9.0 assumes the

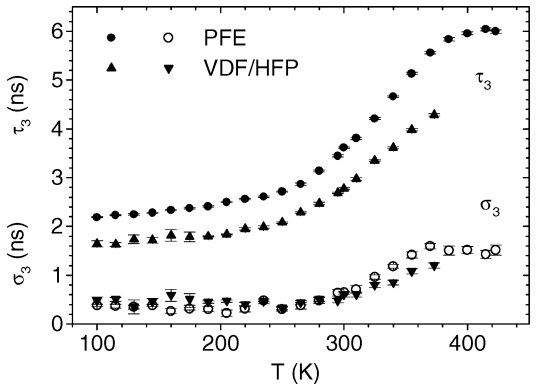

Figure 9. The o-Ps lifetime, τ_3, and its dispersion, σ_3, for PFE (circles) and VDF/HFP_{22} (triangles, mode iv of analysis).

annihilation rate distribution $\alpha_i(\lambda)$ of the ith annihilation channel to be a log−normal function and determines from the fits to the spectra the position of the maximum of the distribution, λ_{i0}, and the standard deviations, $\sigma_i(\lambda)$.[23,24] The mean o-Ps lifetime, τ_3, is related to λ_{30} via $\tau_3 = \exp[\sigma_3^2(\lambda)/2]/\lambda_{30}$ and the dispersion in the o-Ps lifetime distribution, σ_3, via $\sigma_3 = \sigma(\tau_3) = \tau_3\{\exp[\sigma_3^2(\lambda)] - 1\}^{0.5}$.

With eq 5 and the known distribution $\alpha_3(\lambda)$ of the o-Ps annihilation rates the hole radius probability distribution, $n(r_h) = -\alpha_3(\lambda)\mathrm{d}\lambda_3/\mathrm{d}r_h$, can be calculated from[11,12]

$$n(r_h) = -3.32\{\cos[2\pi r_h/(r_h + \delta r)] - 1\}\alpha_3(\lambda)/(r_h + \delta r)^2 \quad (6)$$

The fraction of the free volume holes with radii between r_h and $r_h + \mathrm{d}r_h$ is $n(r_h)\mathrm{d}r_h$. From eq 6 the volume fraction hole size distribution

$$g(v_h) = n(r_h)/4\pi r_h^2 \quad (7)$$

and the number fraction hole size distribution

$$g_n(v_h) = g(v_h)/v_h \quad (8)$$

can be calculated. $g(v_h)$ gives the volume fraction of free volume holes with volume between v_h and $v_h + \mathrm{d}v_h$, while $g_n(v_h)$ shows the number fraction of holes with volume between v_h and $v_h + \mathrm{d}v_h$. The normalization of the distributions is $\int g(v_h)\,\mathrm{d}v_h = \int v_h g_n(v_h)\,\mathrm{d}v_h = \langle v_h\rangle N_h = h$, where $\langle v_h\rangle$ and N_h are the mean volume and mean number density of holes. The values r_h and v_h describe now the size of individual holes, while $\langle v_h\rangle$ denotes the mean, number-averaged hole volume. The distribution $g_n(v_h)$ may be approximated by a log−normal function, a Γ-function, or more roughly by a Gaussian in agreement with the theoretical considerations of Robertson[4] and Bueche.[44] We have calculated the mean, $\langle v_h\rangle$, and the variance, σ_h^2, of the hole size distribution numerically as first and second moment of the $g_n(v_h)$ distribution.

In the next section we will show that there are indications that o-Ps may possibly prefer larger holes. Assuming that this preference can be described by a weighting factor proportional to the hole volume v_h, the distribution $g_n(v_h)$ calculated from $\alpha_3(\lambda)$ is to consider rather as a volume fraction than a number fraction hole size distribution. To come to the true number fraction distribution, which we denote by $g_n(v_h)^*$, the distribution $g_n(v_h)$ must be weighted with $1/v_h$, $g_n(v_h)^* = g_n(v_h)/v_h$. The mean and the variance of $g_n(v_h)^*$, $\langle v_h\rangle^*$, and σ_h^{*2}

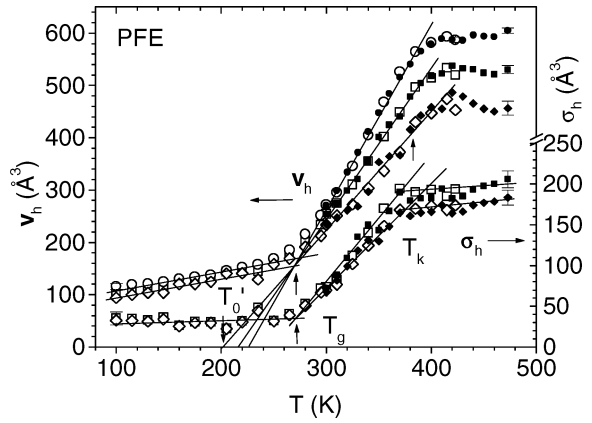

Figure 10. Mean hole volume $\boldsymbol{v}_h$ for PFE calculated either as $\boldsymbol{v}_h = v_h(\tau_3)$ (circles), the number-average, $\langle v_h \rangle$, of the hole volume distribution $g_n(v_h)$ (squares), or the corrected average volume $\langle v_h \rangle^*$ calculated from the modified distribution $g_n(v_h)^* = g_n(v_h)/v_h$ (diamonds) and the corresponding hole volume dispersions $\boldsymbol{\sigma}_h = \sigma_h$ and σ_h^* as a function of the temperature, T. Empty symbols: virgin sample; filled symbols: a second sample after annealing in a vacuum at 120 °C for 4 h. T_g and T_k denote the glass transition and the "knee" temperature (see text); T_0' is the temperature where the hole volume, extrapolated form the rubbery state, disappears. The straight lines are due to linear fits.

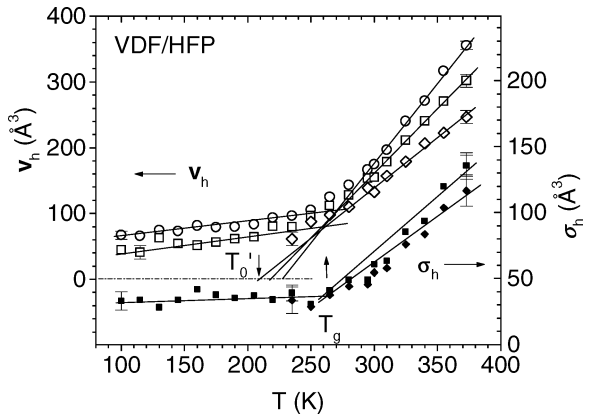

Figure 11. As in Figure 10, but VDF/HFP_{22}.

will be calculated, as before, numerically as first and second moment of this distribution.

Figures 10 and 11 show for PFE and VDF/HFP_{22} plots of the mean hole volume, which we denote by the bold symbol $\boldsymbol{v}_h$, calculated either as $\boldsymbol{v}_h = v_h(\tau_3)$, $\langle v_h \rangle$, or $\langle v_h \rangle^*$, and the corresponding hole volume dispersions, $\boldsymbol{\sigma}_h = \sigma_h$ and σ_h^*. All values show a typical glass transition behavior: they increase slightly or are constant below T_g, but exhibit a strong increase above. As can be observed, $\langle v_h \rangle^*$ is generally smaller than $\langle v_h \rangle$, and this is smaller than $v_h(\tau_3)$. The same is true for the slopes of these mean volumes above T_g and for the dispersions σ_h^* and σ_h. This behavior is due to the weightings of the distributions with $1/v_h$. (The volume-averaged hole size, i.e., the mean of $g(v_h)$, behaves like $v_h(\tau_3)$ and is only slightly larger.) The ratios $\langle v_h \rangle / v_h(\tau_3)$ and $\langle v_h \rangle^* / v_h(\tau_3)$ decrease with increasing ratio σ_3/τ_3 and decreasing τ_3. For $\tau_3/\sigma_3 = 0.25$ and $\tau_3 = 6.0$ ns ratios of 0.88 and 0.78 are found where for $\tau_3 = 2.0$ ns these ratios are 0.80 and 0.59, respectively.

VDF/HFP_{22} (Figure 11) shows a similar behavior to PFE except that the hole volumes are smaller. For the temperature range below T_g we have not shown in Figure 11 the values of $\langle v_h \rangle^*$ (and σ_h^*) but assumed that they agree with those of $\langle v_h \rangle$. The reason for doing this is the following complication. For small values of τ_3 and not too small values of σ_3 the left wing of the o-Ps lifetime distribution may extend to lifetimes below 0.5 ns. Equation 5, however, assumes the inverse of the spin-averaged o-Ps annihilation rate, 0.5 ns, as minimum o-Ps lifetime for a hole radius of $r_h \rightarrow 0$. This causes nonzero values and a breaking off of the calculated distribution for $r_h \rightarrow 0$ as well as wrongly calculated average volumes. The effect is strongest in $\langle v_h \rangle^*$ since the weight $1/v_h$ in the distribution enhances the values for small v_h. We have observed this effect in our experiments for VDF/HFP_{22} below T_g and therefore omitted these data in our figure.

The general behavior of the mean hole volume shown in Figures 10 and 11 corresponds to that known for other polymers apart from the rather large hole sizes. These are, however, typical for fluorine polymers.[45−47] In polystyrene (PS, T_g = 372 K), for example, $v_h(\tau_3)$ changes from 80 Å^3 at 100 K to 220 Å^3 at 473 K.[21] In semicrystalline poly(tetrafluoroethylene) (PTFE) 360 Å^3 [45,46] and in a glassy TFE copolymer (Teflon AF1400) ∼460 Å^3,[47] both values at 300 K, have been found.

At low temperatures, o-Ps atoms are trapped in local free volumes within the glassy matrix, and the o-Ps lifetime mirrors the size of static holes. The averaging occurs over the hole sizes and shapes. The slight increase of $\boldsymbol{v}_h$ with temperature mirrors the thermal expansion of free volume in the glass due to the anharmonicity of molecular vibrations and local motions in the vicinity of the holes. In the rubbery state, $T > T_g$, the molecular and segmental mobilities increase rapidly, which lead to a steep rise in the hole size with temperature. Now $\boldsymbol{v}_h$ represents an average value of the local free volumes whose size and shape fluctuate in space and time.

This is obviously not true anymore above a temperature approximately 120 K above T_g, which we have denoted as the "knee" temperature T_k (Figure 10). At this temperature a leveling off of the o-Ps lifetime expansion can be observed. The macroscopic volume shows, as before, a continuous increase. Recently, we have observed for the first time a decrease of σ_h for temperatures above T_k when studying polycaprolactone.[36] This behavior must be related to the nature of the leveling off of τ_3. In the literature different possible reasons for knee behavior are discussed. One of these could be that the structural relaxation time reaches the order of the o-Ps lifetime of ∼6 ns, leading to a smearing of holes during the life of o-Ps.[36]

From linear least-squares fits in the temperature ranges between 120 and 235 K and 300 and 380 K (295−373 K for VDF/HFP_{22}) the value of T_g, the mean hole volume at T_g, $\boldsymbol{v}_{hg}$, and the coefficient of thermal expansion of holes, $\alpha_h = (1/\boldsymbol{v}_{hg})d\boldsymbol{v}_h/dT$, are estimated. The data are shown in Table 2 (g = glassy state, r = rubbery state). α_h of both fluoroelastomers is distinctly larger than that of PS, for example (PS: $\alpha_h = [1/v_h(\tau_3)]dv_h(\tau_3)/dT = 9.26 \times 10^{-3}$ K^{-1}).[21] The α_h values are larger by a factor of 18−25 than those of the macroscopic coefficient of thermal expansion, α ($T > T_g$). The results for VDF/HFP_{22} are qualitatively similarly to those of PFE and do not need an extra discussion. We remark that the coefficient of thermal expansion of the hole volume is 18−25 times larger than that of the macroscopic volume. That is what we expect if the thermal expansion takes

Table 2. Free Volume Parameters Estimated from the PALS Data

quantity	uncertainty	PFE	VDF/HFP$_{22}$
T_g (PALS, K)[c]	±5	265	260
T_0' (PALS, K)[c]	±10	203	209
$\langle v_{hg}\rangle$ (Å^3)[a]	±2	170.1	101.7
$\langle v_{hg}\rangle$ (Å^3)[b]	±3	162.5	84.2
$\langle v_{hg}\rangle$ (Å^3)[c]	±5	153.0	84.9
α_{hg} (10^{-3} K^{-1})[a]	±0.07	2.09	2.14
α_{hg} (10^{-3} K^{-1})[b]	±0.1	2.18	3.13
α_{hg} (10^{-3} K^{-1})[c]	±0.13	2.25	∼3.1
α_{hr} (10^{-3} K^{-1})[a]	±0.1	20.9	24.4
α_{hr} (10^{-3} K^{-1})[b]	±0.15	17.8	23.5
α_{hr} (10^{-3} K^{-1})[c]	±0.2	14.9	18.0
N_h' (from V_f, 10^{21} g^{-1})[a]	±0.006	0.131	0.180
V_{f0} (cm^3/g)[a]	±0.002	0.015	0.010
N_h' (from V_f, 10^{21} g^{-1})[b]	±0.008	0.161	0.223
V_{f0} (cm^3/g)[b]	±0.0025	0.011	0.006
N_h' (from V_f, 10^{21} g^{-1})[c]	±0.01	0.199	0.286
V_{f0} (cm^3/g)[c]	±0.003	0.007	0.002
N_h' (from V) (10^{21} g^{-1})[a]	±0.006	0.129	0.172
V_{occ} (cm^3/g)	±0.002	0.447	0.525
N_h' (from V) (10^{21} g^{-1})[b]	±0.008	0.157	0.2121
V_{occ} (cm^3/g)	±0.0025	0.443	0.522
N_h' (from V) (10^{21} g^{-1})[c]	±0.01	0.195	0.272
V_{occ} (cm^3/g)	±0.003	0.439	0.518
N_h (nm^{-3})[c]	±0.01	0.41	0.52
$1/N_h$ (nm^3)[c]	±0.1	2.4	1.9

[a] From $v_h(\tau_3)$. [b] From $\langle v_h\rangle$. [c] From $\langle v_h\rangle$*; see text.

place predominantly in the excess free volume which is only 5−10% of the total volume (at T_g).

The linear extrapolation of the mean hole volume from the rubbery state down to $\boldsymbol{v_h} = 0$ delivers the temperature T_0' (Figures 10 and 11, Table 2). The lowest T_0' values are obtained from the fits to $\langle v_h\rangle$*. This values are larger than those found from the parabolic fits to the specific free volume V_f (Figures 3 and 4, Table 1). Unfortunately, the $\boldsymbol{v_h}$ data are not sufficiently accurate for nonlinear fits. Linear fits to V_f deliver almost the same T_0' values than obtained from $\langle v_h\rangle$*.

The Hole Density. An estimate of the hole density may be obtained by comparing PALS and PVT experiments. The mean number of holes per mass unit, N_h', may be determined from one of the relations[15]

$$V_f = V_{f0} + N_h'\boldsymbol{v}_h \tag{9}$$

$$V = V_{occ} + V_{f0} + N_h'\boldsymbol{v}_h \tag{10}$$

where $\boldsymbol{v}_h = v_h(\tau_3)$, $\langle v_h\rangle$, or $\langle v_h\rangle$*. In these equations, the free volume V_f estimated from the S−S eos analysis of PVT data, $V_f = hV$, is expressed by $N_h'\boldsymbol{v}_h$. The term V_{f0} may count for a possible deviation of the mean hole volume estimated from the o-Ps lifetime data from the true mean hole volume.[17,19] Figures 12 and 13 show the specific free volume, $V_f = hV$, and the specific total volume, V, both plotted vs the mean hole volume $\boldsymbol{v}_h$ for PFE and VDF/HFP$_{22}$. The data were taken from the temperature range between T_g + 30 K and T_k. One observes that both volumes V_f and V follow linear functions of $\boldsymbol{v}_h$. From this behavior it is concluded that N_h' is not a function of the temperature. The slope of the V_f vs $\boldsymbol{v}_h$ curves, which corresponds directly to N_h', increases when going from $v_h(\tau_3)$ to $\langle v_h\rangle$ and $\langle v_h\rangle$* while the value V_{f0} decreases (Table 2). Assuming that the slope of the curves is correct, values of V_{f0} being larger than zero may be interpreted as due to an underestimation of the true mean hole size, v_h^{true}, by PALS by a value of $\boldsymbol{v}_{h0}$, $\boldsymbol{v}_h = \boldsymbol{v}_h^{PALS} = v_h^{true} - \boldsymbol{v}_{h0}$ and $V_{f0} = N_h'\boldsymbol{v}_{h0}$.

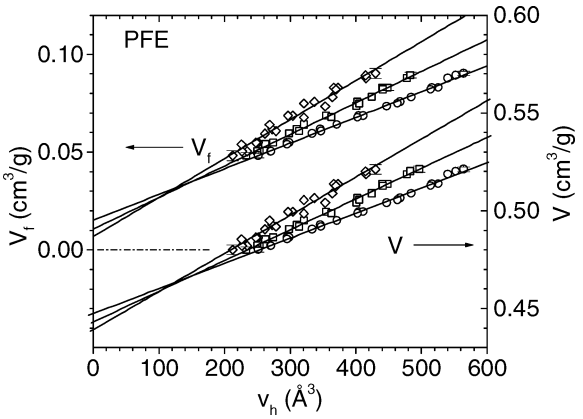

Figure 12. Specific free volume V_f and specific total volume V plotted vs the mean hole volume calculated as $\boldsymbol{v}_h = v_h(\tau_3)$ (circles), $\langle v_h\rangle$ (squares), or $\langle v_h\rangle$* (diamonds) for PFE (see text). The lines show linear fits to the data from the temperature range between T_g + 30 K and T_k.

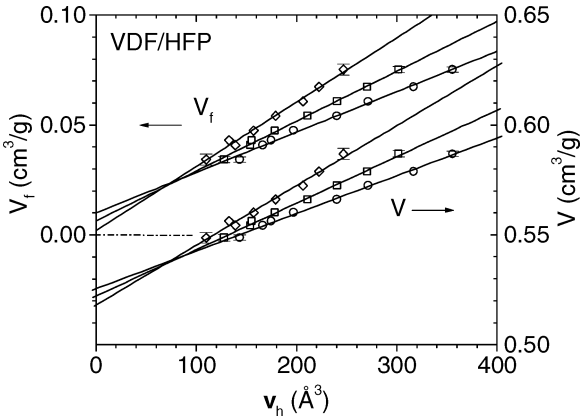

Figure 13. As in Figure 12, but for VDF/HFP$_{22}$.

This effect may occur since nonspherical holes are detected by o-Ps as too small holes.[8,48,49] The estimated values of $\boldsymbol{v}_{h0} = v_{h0}(\tau_3) = 116$ Å^3 and $\boldsymbol{v}_{h0} = \langle v_{h0}\rangle = 66$ Å^3 (for PFE), however, seem to be unrealistically high.

Another possible explanation could be that the hole size is increasingly overestimated with increasing temperature. This would lead to a too small slope of the V_f vs $\boldsymbol{v}_h$ curves. This effect could be caused by a preference of larger holes by o-Ps which might be thermally assisted. Energetic reasons for this possible effect[50] and corresponding computer simulations[51] can be found in the literature. Although the mean diffusion length of o-Ps is small (∼2 nm[52]), this effect could lead to the detection of a more or less volume weighted hole size distribution. As discussed previously, we have calculated the distribution $g_n(v_h)^* = g_n(v_h)/v_h$ in order to correct this possible effect. Its mean volume, $\langle v_h\rangle$*, shows the lowest value of $V_{f0} = 0.0068$, which corresponds to $\langle v_{h0}\rangle^* = 34.4$ Å^3 (PFE). This value seems to be acceptable. Our conclusion that $\langle v_h\rangle$* may correspond best to the true mean hole size needs further support by evidence. Therefore, we have shown in our figures and in Table 2 the results of all the three ways of calculating a mean hole volume $\boldsymbol{v}_h$. The estimated values for the specific hole number $N_h' = 0.131 \pm 0.006$ ($v_h(\tau_3)$), 0.161 ± 0.008 ($\langle v_h\rangle$), and 0.199 ± 0.01 ($\langle v_h\rangle$*) in units of 10^{21} g^{-1} of PFE correspond to volume-related hole number densities, $N_h = N_h'/V$, of $N_h = 0.26$, 0.32, and 0.39 in units of nm^{-3}. For VDF/HFP$_{22}$ N_h' values larger by a factor of ∼1.5 than for PFE are observed.

These values can be compared with those estimated for PS,[20,21] for example, $N_h' = 0.53 \times 10^{21}$ g^{-1} and $N_h = 0.55$ nm^{-3}. Srithawatpong et al.[16] observed for a series of polymers increasing values of $v_h(\tau_3)$ and N_h' at T_g with increasing value of T_g. Our results for PFE show that the hole volume at T_g has here an extraordinarily large value. This is probably caused by the perfluoro(methyl vinyl ether) comonomer which prevents dense packing.

The plots of the specific (total) volume, V, vs the three different mean hole volumes, $\boldsymbol{v_h}$, deliver slightly, but systematically larger slopes than found from the V_f vs $\boldsymbol{v_h}$ plots: 0.133, 0.162, and 0.202 in units of 10^{21} g^{-1} for PFE. For calculation of N_h' the slope $dV/d\boldsymbol{v_h}$ must be corrected by the expansion of the occupied volume, $N_h' = dV/d\boldsymbol{v_h} - dV_{occ}/d\boldsymbol{v_h}$. This correction is very small since $dV_{occ}/d\boldsymbol{v_h} = (dV_{occ}/dT)/(d\boldsymbol{v_h}/dT) = \alpha_{occ}V_{occ}/\alpha_h\boldsymbol{v_h} = 0.0036$, 0.0049, and 0.0073 in units of 10^{21} g^{-1} for $v_h(\tau_3)$, $\langle v_h\rangle$, and $\langle v_h\rangle$*, respectively. The N_h' values estimated by applying this correction agree very well with those from the V_f vs $\boldsymbol{v_h}$ plots (Table 2). The zero volumes, $V(\boldsymbol{v_h} = 0)$, correspond to $V_{occ} + V_{f0}$ where for all of the three plots identical values of $V_{occ} = 0.432$ cm^3/g were found using the V_{f0} values of the V_f vs $\boldsymbol{v_h}$ plots (Table 2). This value agrees with that obtained directly from the S−S eos analysis, $V_{occ} = 0.431$ cm^3/g (300 K). In estimating N_h' the value of dV_{occ}/dv_h cannot be neglected at temperatures below T_g and generally not for isothermal compression experiments.[20,21] The reason is that, as shown in one of the preceding sections, the compressibility of the occupied volume, κ_{occ}, cannot be neglected in comparison with that of the total volume, κ. Taking this into account, the discrepancy in the estimation of the hole density from thermal expansion and isothermal compression experiments which has been observed by Bohlen and Kirchheim[18] appears to be due to the incorrect assumption $\kappa_{occ} = 0$ made in their paper.

The Hole Size Distribution and the S−S Model. It is rather satisfactory that the simple phenomenological formula eq 10 gives the same results for N_h' as eq 9 which uses the advanced S−S eos theory for the calculation of V_f. It shows that both methods detect the same quantity of excess free volume and its variation with the temperature. However, there seems to exist a discrepancy between the free volume structures as observed by PALS and the modeling underlying the S−S eos. o-Ps detects holes which have a size distribution around a mean value. The mean hole size and the width of the distribution increase with increasing temperature while the mean hole number is estimated to be constant. The S−S model, on the other hand, assumes uniform cells of a size which increases only weakly with the temperature. The increase in free volume comes mainly from the creation of new empty cells.[3−5] Moreover, the holes from PALS are much larger than the empty cell size from S−S theory.

This discrepancy can be resolved employing results of Vleeshouwers et al.,[6] who assumed that the holes probed by o-Ps represent agglomerates of unoccupied cells described by the S−S theory. These authors performed Monte Carlo simulations to obtain the agglomerate size distribution as a function of the hole fraction $h(T)$ assuming a random distribution of empty lattice cells. The MC results were represented by the empirical function

$$p_i = p_n \exp[-(i/l(y))^{\beta(y)}] \quad \text{for } 0.8 \le y \le 0.99 \qquad (11)$$

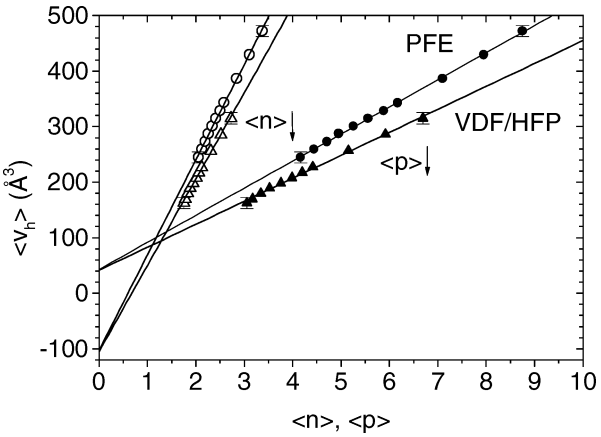

Figure 14. Plot of the number-averaged mean hole volume, $\langle v_h\rangle$, from PALS vs the volume-averaged ($\langle p\rangle$, filled symbols) and the number-averaged ($\langle n\rangle$, empty symbols) mean size of clusters. The clusters size is given as number of empty cells of the S−S lattice within a cluster. Circles: PFE; triangles: VDF/HFP$_{22}$.

where the quantity p_i is defined as the fraction of free volume present in agglomerates which contain i vacant lattice sites and p_n is a normalization factor, so that $\sum p_i = 1$. $l(y)$ and $\beta(y)$ are a linear and a quadratic function of the occupation fraction $y = 1 - h$ (eqs 8 and 9 in ref 6). The number fraction of vacancy clusters of size i can be calculated via

$$n_i = (p_i/i)/(\sum p_i/i) \qquad (12)$$

Figure 14 shows for PFE and VDF/HFP$_{22}$ the number-averaged hole volume, $\langle v_h(T)\rangle$, which was calculated from PALS experiments using eq 8, plotted vs the volume-averaged, $\langle p[h(T)]\rangle$, and the number-averaged cluster size, $\langle n[h(T)]\rangle$. $\langle p\rangle$ and $\langle n\rangle$ were calculated as the first moment of the distributions given by eqs 11 and 12, where $i = 1.30$. $\langle v_h\rangle$ follows linear functions of $\langle n\rangle$ and $\langle p\rangle$ with constants of $A_0 = -102 \pm 5$ Å^3, $A_1 = 173.1 \pm 2$ Å^3 and $A_0 = 42.9 \pm 2$ Å^3, $A_1 = 48.8 \pm 0.5$ Å^3, respectively, for PFE and $A_0 = -105 \pm 6$ Å^3, $A_1 = 155.4 \pm 3$ Å^3 and $A_0 = 41.6 \pm 3$ Å^3, $A_1 = 41.4 \pm 0.7$ Å^3, respectively, for VDF$_{78}$/HFP$_{22}$.

For a complete correspondence of PALS with the S−S theory we expect $A_0 = 0$ and $A_1 = \omega$ where, as before, ω is the S−S theory cell size estimated previously to be $\omega = 45.2$ Å^3 for PFE and $\omega = 45.9$ Å^3 for VDF/HFP$_{22}$. We observe that the plot of $\langle v_h\rangle$ vs $\langle p\rangle$ agrees much better with this expectation than $\langle v_h\rangle$ vs $\langle n\rangle$. This behavior supports our previous conclusion that o-Ps may prefer larger holes with a weight of approximately "v_h". The nonvanishing value of A_0 may be easily caused by a slightly different weight in the distribution than assumed.

The observation of a temperature independent specific hole number, N_h', seems to be unexpected, although it is confirmed by all other related work in the literature.[13−21] We can explain this mystery in terms of the S−S theory considering the relations $V_f = hV = N_h'\langle v_h\rangle^* = N_h^{SS}\omega$ and $\langle v_h\rangle^* = \langle n\rangle\omega$. From these follows $N_h' = N_h^{SS}/\langle n\rangle = (hV/\omega)/\langle n\rangle = (h/y)(V_{occ}/\omega)/\langle n\rangle$. Since (V_{occ}/ω) is a constant, the constancy of N_h' requires a constant ratio $(h/y)/\langle n\rangle$. We found that the ratio $(h/y)/\langle n\rangle$ follows an almost linear function but with a very small increase, $(h/y)/\langle n\rangle = 0.0455 + 3.0 \times 10^{-5}T$ for PFE and $(h/y)/\langle n\rangle = 0.040 + 3.9 \times 10^{-5}T$ for VDF/HFP$_{22}$. From this behavior we conclude that, in terms of the S−S theory,

the constancy of N_h' observed in PALS experiments comes from the similar temperature dependencies of (h/y) and $\langle n \rangle$.

Hole Size Distribution and Thermal Volume Fluctuation. Because of thermal fluctuations, the volume V occupied by a fixed number of molecules is not the same at all points in time and space, it fluctuates around a mean value.[4] The corresponding density fluctuations can be observed in small-angle X-ray scattering (SAXS) experiments.[53,54] These fluctuations correspond to fluctuations in the local free volume which are mirrored by PALS. PALS detects these fluctuations as a quasi-static hole size distribution as long as the relaxation times for segmental motion are larger than the o-Ps lifetime of 2−6 ns. The root-mean-square fluctuation in the fractional free volume can be estimated from the PALS data via

$$\delta \boldsymbol{f}_{\mathbf{rms}} = (\langle \delta V_f{}^2 \rangle / \langle V \rangle^2)^{1/2} = (\langle N_h' \rangle / \langle V \rangle) \boldsymbol{\sigma}_{\mathbf{h}} \qquad (13)$$

where $\langle \delta V_f{}^2 \rangle = \langle (V_f - \langle V_f \rangle)^2 \rangle$ is the variance of the specific volume fluctuation. The right-hand side of eq 13 comes from the assumption that the holes detected by PALS have a distribution only in size but not in number ($\langle \delta N_h'^2 \rangle = 0$). This assumption is justified by the temperature independence of N_h'. $\boldsymbol{\sigma}_{\mathbf{h}}{}^2 = \langle \delta \nu_h{}^2 \rangle = \langle (\nu_h - \langle \nu_h \rangle)^2 \rangle$, where $\langle \nu_h \rangle = \boldsymbol{\nu}_h = \langle \nu_h \rangle$ and $\langle \nu_h \rangle^*$, is the variance of the hole volume fluctuation which is displayed in Figures 10 and 11 as $\boldsymbol{\sigma}_{\mathbf{h}} = \sigma_h$ and $\sigma_h{}^*$. Figure 15 shows the variation of $\delta \boldsymbol{f}_{\mathbf{rms}}$ for the temperature range 200 K $< T < T_k$. The data below T_g are shown for the illustration of the behavior of $\delta \boldsymbol{f}_{\mathbf{rms}}$ in the glass. They are calculated from eq 13 with the approximation $V(T < T_g) = V(T_g)$.

Following conventional thermodynamics,[4] the mean-square fluctuation of the volume V about its mean value $\langle V \rangle$ at equilibrium is related to the second derivative of the Helmholtz free energy F via $\langle \delta V^2 \rangle = -k_B T/(\mathrm{d}^2 F/\mathrm{d}V^2)_{\langle V \rangle}$. With $(\mathrm{d}^2 F/\mathrm{d}V^2)_{\langle V \rangle} = -(\mathrm{d}P/\mathrm{d}V)_{\langle V \rangle}$ one obtains the well-known relation $\langle \delta V^2 \rangle = k_B T \kappa \langle V \rangle$. Assuming that the fluctuation in the free and occupied volume are independent, $\langle \delta V^2 \rangle = \langle \delta V_f{}^2 \rangle + \langle \delta V_{occ}{}^2 \rangle$, one obtains for the fractional free volume fluctuation

$$\delta f_{rms} = (k_B T \kappa_f \langle V_f \rangle / \langle V \rangle^2)^{1/2} = (k_B T \kappa_f{}^* / \langle V \rangle)^{1/2} \qquad (14)$$

where $\kappa_f = (1/\langle V_f \rangle)(\mathrm{d}\langle V_f \rangle/\mathrm{d}P)_T$ is the compressibility of the free volume and $\kappa_f{}^* = (1/\langle V \rangle)(\mathrm{d}\langle V_f \rangle/\mathrm{d}P)_T = h\kappa_f$ is the corresponding fractional compressibility. For a rough estimation $\kappa_f{}^* = \kappa - \kappa_{occ}{}^*$ ($\kappa_{occ}{}^* \approx \kappa_{occ}$) may be substituted by κ or by the difference of the values of κ above and below T_g. In the current work we have, however, calculated the correct value of $\kappa_f{}^*$ from the data of our S−S eos analysis.

Thermal fluctuations are considered in a subvolume $\langle V \rangle$ embedded in, and being in thermodynamic contact with, a much larger one. $\langle V \rangle$ must be now chosen as the volume in which the fluctuations are desired.[4] Figure 15 shows the behavior of δf_{rms} which was calculated from eq 14 assuming that the fluctuation volume is constant and equal to the volume which contains one hole; for PFE $\langle V \rangle = 1/N_h = 3.1$ nm^3 ($N_h = 0.32$ nm^{-3}, from $\langle \nu_h \rangle$, dotted line) and $\langle V \rangle = 1/N_h = 2.5$ nm^3 ($N_h = 0.39$ nm^{-3}, from $\langle \nu_h \rangle^*$, dashed line). δf_{rms} increases above T_g with the temperature due to the increase of $\kappa_f{}^*$ and T in eq 14; however, the increase is distinctly too small compared with the PALS data. The same behavior can be observed for VDF/HFP$_{22}$. To resolve this discrepancy, we take into account that the subvolume $\langle V \rangle$ has a similar meaning than the cooperative rearranging region (CRR) in the theories of dynamic heterogeneity of glass-forming liquids.[55,56] The CCRs constitute a cell structure which is representative for the given polymer and with structural and dynamic heterogeneity inside the cells. The inner part of the CRR is assumed to have lower density and higher mobility (the Glarum−Levey defect; see Donth[56] and references given therein). It is surrounded by (fluctuating in space and time) cell walls of lower mobility and higher density. In the framework of the fluctuation approach to the glass transition by Donth,[56] it has been calculated from heat capacity spectroscopy data that the size of the CRR at T_g is typically a few nm^3. Domains of similar size were detected in nuclear magnetic resonance experiments by Spiess and collaborators.[57] The size decreases with increasing temperature, and the heterogeneity disappears at a critical (onset or cross over) temperature $T_c > T_g$.

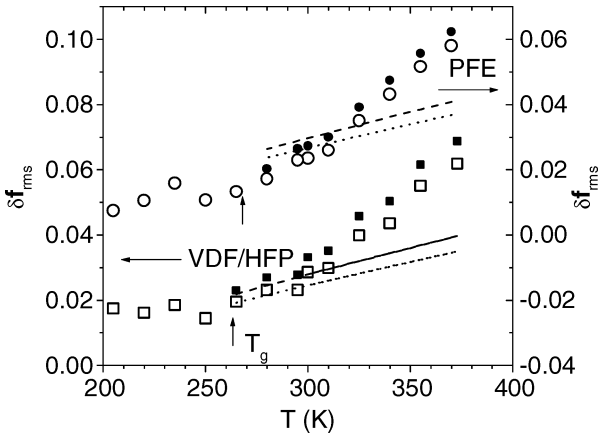

Figure 15. Root-mean-square fluctuation of the fractional free volume, $\delta \boldsymbol{f}_{rms}$, derived from the PALS data of PFE (circles) and VDF/HFP$_{22}$ (squares) either from σ_h (empty symbols) or from $\sigma_h{}^*$ (filled symbols). The dotted and dashed lines show $\delta \boldsymbol{f}_{rms}$ calculated from the thermodynamic fluctuation theory with constant fluctuation volume $\langle V \rangle = 1/N_h$. The statistical errors of experiments are of ±0.005; dotted line: N_h from $\langle \nu_h \rangle$; dashed line: N_h from $\langle \nu_h \rangle^*$ (see Table 2).

Possibly, the hole detected by o-Ps may be considered as the inner part of the CRR (the Glarum−Levey defect), and the fluctuation volume may be identified with a CRR. Following this philosophy, we have calculated a variable value $\langle V \rangle$ so that eq 14 fits the PALS data. The results of our calculation are shown in Figure 16. In the case of PFE, $\langle V \rangle$ decreases from 3.0 nm^3 (for $\sigma_h{}^*$ and 3.9 nm^3 for σ_h) at 300 K to 1.0 (1.2) nm^3 at $T_k = 380$ K. The curve may be fitted by a function of the type $\langle V \rangle = a(b + T)/(c + T)$ (shown) or an exponential function. The extrapolation to $T = T_g \approx 270$ K leads to a value of $\langle V \rangle \approx 5.8$ (7.2) nm^3. These volumes correspond to a number of s-mers or cells of the S−S lattice, $\langle V \rangle/\omega$, between 116 (144) at T_g and ∼20 at T_k. This number might be interpreted as the cooperativity[56] of the system. In the case of VDF/HFP$_{22}$, the estimated fluctuation volumes are distinctly smaller than for PFE and vary between ∼2 nm^3 at T_g and 0.7 nm^3 at 380 K.

Our fluctuation volume corresponds in size and temperature dependence closely to the behavior of the CRR as derived from calorimetric data. The (almost) constancy of $1/N_h$ but the distinct decrease of $\langle V \rangle$ with increasing temperature may be explained by assuming

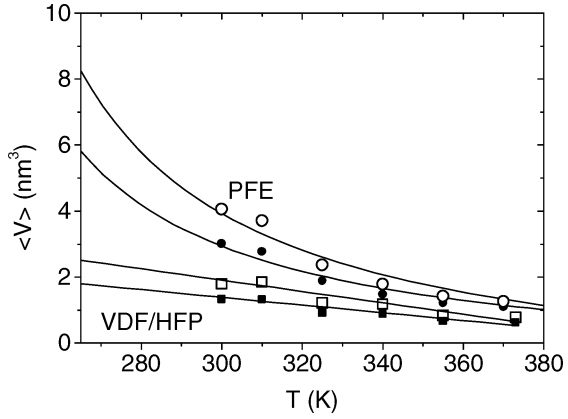

Figure 16. Variation of the fluctuation volume $\langle V \rangle$ estimated from the data shown in Figure 15.

that the CRRs fill completely the entire volume only at T_g ($\langle V(T_g) \rangle = 1/N_h$) but form in the temperature range $T > T_g$ a constant number (equal to N_h) of regions of decreasing size (equal to $\langle V(T) \rangle$). There are several other points where correlations between the theory of dynamic heterogeneity of glass-forming liquids and PALS results may be realized. The correlation between T_0' and the Vogel temperature T_0 has been previously determined.[58,59] The o-Ps knee temperature T_k may correspond to the critical temperature T_c where the dynamic heterogeneity of the system disappears,[59,60] and the fragility of the liquids seem to correlate with their thermal expansivity.[61]

Conclusions

1. The PVT curves of PFE and VDF/HFP$_{22}$ can be well fitted by the S−S eos in the temperature range between 27 and 200 °C and pressure range between 0 and 200 MPa. From the S−S eos the fraction of holes (empty lattice sites), which constitute the excess free volume, is estimated for PFE to vary between 0.099 (300 K) and 0.23 (473 K). This corresponds to a variation of the specific free volume $V_f = hV$ between 0.05 and 0.13 cm^3/g. The hole fraction h follows an Arrhenius law with an activation enthalpy approximately half of the cohesive energy. The coefficient of thermal expansion and the compressibility of the free volume are more than 1 order of magnitude larger than those of the total volume V. The occupied volume, $V_{occ} = (1 - h)V$, shows a very small thermal expansion but a distinct compressibility (all above T_g). From this it follows that for a given total volume V, the excess free volume V_f is not constant but depends on the route in the $T-P$ plane on which V is reached.

2. A correct analysis of the positron lifetime spectra requires the dispersion in both the o-Ps lifetime τ_3 and the e^+ lifetime τ_2 to be taken into account. This can be successful done employing the analysis routine LT9.0. In that case the theoretically expected parameters of the p-Ps annihilation come out of the analysis, and the e^+ lifetime τ_2 shows a strongly reduced response to the glass transition. Probably, positrons annihilate in both the interstitial free volume (inherent to each lattice cell) and the excess free volume (empty lattice cells), while the Ps "atom" is formed and localized only in the excess free volume.

3. A correct estimation of the mean size of the holes in which o-Ps annihilates requires the calculation of the mass center $\langle v_h \rangle$ of the number fraction hole volume distribution $g_n(v_h)$. A direct calculation from τ_3, $v_h(\tau_3)$, provides too large values. Some indications were found that o-Ps may prefer larger holes with a weight approximately proportional to the hole volume. A good measure for the true mean hole volume may be therefore the mass center $\langle v_h \rangle^*$ of the corrected distribution $g_n(v_h)^* = g_n(v_h)/v_h$. Further research is, however, necessary to confirm this conclusion. The mean hole size and the hole size dispersion increase strongly above T_g with the temperature, while the specific hole density N_h', calculated from a comparison of V_f or V with $\langle v_h \rangle^*$ or $\langle v_h \rangle$, is constant.

Apparent discrepancies between the S−S modeling and the results from PALS can be resolved assuming that the holes in which o-Ps annihilates represent agglomerates of the empty cells described by the S−S theory. Within this line the temperature independence of PALS hole (agglomerate) density N_h' can be explained. Attempts have been made to interpret the PALS results in terms of the Vogel, glass transition, and critical temperatures, cooperative rearranging region (CRR), its temperature-dependent size and cooperativity, and the Glarum−Levey defect employed in the theory of structural and dynamic heterogeneity of glass-forming liquids.

In a subsequent work we study the pressure dependence of the free volume of the fluoroelastomers and present further confirmations of the conclusions of this paper.

Acknowledgment. We thank D. Kilburn/Bristol for critical reading of the manuscript and J. Kansy/Katowice for delivering the new routine LT9.0 and stimulating discussions to the subject. R. Simha/Cleveland is gratefully acknowledged for the stimulation discussion to the S−S eos. A.S.G. thanks the Deutscher Akademischer Ausstauschdienst and the Martin-Luther-University Halle-Wittenberg for support as a visiting scientist.

References and Notes

(1) Améduri, B.; Boutevin, B.; Kostov, G. *Prog. Polym. Sci.* **2001**, *26*, 105.
(2) Hougham, G., Cassidy, P. E., Johns, K., Davidson, T., Eds.; *Fluoropolymers 2*: *Properties*; Kluwer Academic/Plenum Publishers: New York, 1996.
(3) Simha, R.; Somcynsky, T. *Macromolecules* **1969**, *2*, 342.
(4) Roberson, R. E. In *Computational Modeling of Polymers;* Bicerano, J., Ed.; Marcel Dekker: Midland, MI, 1992; p 297.
(5) Utracki, L. A.; Simha, R. *Macromol. Theory Simul.* **2001**, *10*, 17.
(6) Vleeshouwers, S.; Kluin, J.-E.; McGervey, J. D.; Jamieson, A. M.; Simha, R. *J. Polym. Sci., Part B: Polym. Phys.* **1992**, *30*, 1429.
(7) Schmitz, H.; Müller-Plathe, F. *J. Chem. Phys.* **2000**, *112*. 1040.
(8) Jean, Y. C. *Microchem. J.* **1990**, *42*, 72; in *Positron Annihilation*, Proc. of the 10th Int. Conf., He, Y.-J., Cao, B.-S., Jean, Y. C., Eds.; *Mater. Sci. Forum* **1995**, *175−178*, 59.
(9) Mogensen, O. E. *Positron Annihilation in Chemistry*; Springer-Verlag: Berlin, 1995.
(10) Jean, Y. C., Mallon, P. E., Schrader, D. M., Eds.; *Principles and Application of Positron and Positronium Chemistry*; World Scientific: Singapore, 2003.
(11) Gregory, R. B. *J. Appl. Phys.* **1991**, *70*, 4665.
(12) Liu, J.; Deng, Q.; Jean, Y. C. *Macromolecules* **1993**, *26*, 7149.
(13) Kobayashi, Y.; Zehng, W.; Meyer, E. F.; McGervey, J. D.; Jamison, A.; Simha, R. *Macromolecules* **1989**, *22*, 2302.
(14) Yu, Z.; Yashi, U.; McGervey, J. D.; Jamieson, A. M.; Simha, R. *J. Polym. Sci., Part B: Polym. Phys.* **1994**, *32*, 2637.
(15) Dlubek, G.; Stejny, J.; Alam, M. A. *Macromolecules* **1998**, *31*, 4574.

(16) Srithawatpong, R.; Peng, Z. L.; Olson, B. G.; Jamieson, A: M.; Simha, R.; McGervey, J. D.; Maier, T. R.; Halasa, A: F.; Ishida, H *J. Polym. Sci., Part B: Polym. Phys.* **1999**, *37*, 2754.
(17) Schmidt, M.; Maurer, F. H. J. *Polymer* **2000**, *41*, 8419.
(18) Bohlen, J.; Kirchheim, R. *Macromolecules* **2001**, *34*, 4210.
(19) Dlubek, G.; Bondarenko, V.; Pionteck, J.; Supey, M.; Wutzler, A.; Krause-Rehberg, R. *Polymer* **2003**, *44*, 1921.
(20) Dlubek, G.; Pionteck, J.; Kilburn, D. *Macromol. Chem. Phys.* **2004**, *205*, 500.
(21) Dlubek, G.; Bondarenko, V.; Al-Qaradawi, I. Y.; Kilburn, D.; Krause-Rehberg, R. *Macromol. Chem. Phys.* **2004**, *205*, 512.
(22) Zoller, P.; Walsh, C. J. *Standard Pressure−Volume−Temperature Data for Polymers*; Technomic Publ Co., Inc.: Lancaster, Basel, 1995.
(23) Kansy, J. *Nucl. Instrum. Methods A* **1996**, *374*, 235.
(24) Kansy, J. *LT for Windows, Version 9.0*, Inst. of Phys. Chem. of Metals, Silesian University, Bankowa 12, PL-40-007 Katowice, Poland, March 2002, private communication.
(25) Bondi, A. *J. Phys. Chem.* **1964**, *68*, 441. Bondi, A. *Physical Properties of Molecular Crystals, Liquids, and Gases;* Wiley: New York, 1968; p 450.
(26) Van Krevelen, D. W. *Properties of Polymers*; Elsevier Sci. Publ. Co.: Amsterdam, 1990.
(27) Simha, R.; Wilson, P. S. *Macromolecules* **1973**, *6*, 908.
(28) Jain, R. K.; Simha, R. *J. Polym. Sci., Polym. Lett. Ed.* **1979**, *17*, 33.
(29) Bendler, J. T.; Fontanella, J. J.; Shlesinger, M. F.; Wintersgill, M. C. *Electrochim. Acta* **2003**, *48*, 2267.
(30) Hartmann, B.; Simha, R.; Berger, A. E. *J. Appl. Polym. Sci.* **1991**, *43*, 983.
(31) Perez, J. *Physics and Mechanics of Amorphous Polymers*; A.A. Balkema: Rotterdam, 1998; p 18.
(32) Mark, J. E., Ed.; *Physical Properties of Polymers Handbook*, AIP Press: Woodbury, NY, 1996; Chapter 29.
(33) Dlubek, G.; Eichler, St.; Hübner, Ch.; Nagel, Ch. *Nucl. Instrum. Methods B* **1999**, *149*, 501; *Phys. Status Solidi A* **1999**, *174*, 313.
(34) Gregory, R. B.; Zhu, Y. *Nucl. Instrum. Methods A* **1990**, *290*, 172. Gregory, R. B. *Nucl. Instrum. Methods A* **1991**, *302*, 496.
(35) Shukla, A.; Peter, M.; Hoffmann, L. *Nucl. Instrum. Methods A* **1993**, *335*, 310. Hoffmann, L.; Shukla, A.; Peter, M.; Barbiellini, B.; Manuel, A. A. *Nucl. Instrum. Methods A* **1993**, *335*, 276.
(36) Dlubek, G.; Supej, M.; Bondarenko, V.; Pionteck, J.; Pompe, G.; Krause-Rehberg, R.; Emri, I. *J. Polym. Sci., Part B: Polym. Phys.* **2003**, *41*, 3077.
(37) PATFIT-88: Kirkegaard, P.; Pedersen, N. J.; Eldrup, M. Report RISØ-M-2740, 1989.
(38) Bertolaccini, M.; Bisi, A.; Gambarini, G.; Zappa, L. *J. Phys. C* **1974**, *7*, 3827.
(39) Deng, Q.; Sundar, C. S.; Yean, Y. C. *J. Phys. Chem.* **1992**, *96*, 492.
(40) Starkweather, H. W., Jr.; Zoller, P.; Jones, G. A.; Vega, A. J. *J. Polym. Sci., Polym. Phys. Ed.* **1982**, *751−761*, 751.
(41) Wang, D. L.; Hirade, T.; Maurer, F. H.-J.; Eldrup, M.; Petersen, N. J. *J. Chem. Phys.* **1998**, *108*, 4656.
(42) Tao, S. J. *J. Chem. Phys.* **1972**, *56*, 5499.
(43) Eldrup, M.; Lightbody, D.; Sherwood, J. N. *Chem. Phys.* **1981**, *63*, 51.
(44) Bueche, F. *J. Chem. Phys.* **1953**, *21*, 1850.
(45) Kindl, P.; Puff, W.; Sormann, H. *Phys. Status Solidi A* **1980**, *58*, 489. Kindl, P.; Sormann, H.; Puff, W. In *Positron Annihilation*, Proc. 6th. Int. Conf., Coleman, P. G., Sharma, S. C., Diana, L. M., Eds.; North-Holland Publ. Co.: Amsterdam, 1982; p 685.
(46) Dlubek, G.; Saarinen, K.; Fretwell, H. M. *J. Polym. Sci., Part B: Polym. Phys.* **1998**, *36*, 1513.
(47) Alentiev, A. Yu.; Shantarovich, V. P.; Merkel, T. C.; Bondar, V. I.; Freeman, B. D.; Yamploskii, Y. P. *Macromolecules* **2002**, *35*, 9513.
(48) Jean, Y. C.; Shi, H.; Dai, G. H.; Hunag, C. M.; Liu, L. *Mater. Sci. Forum* **1995**, *175−178*, 691.
(49) Jasinska, B.; Koziol, A. E.; Goworek, T. *J. Radioanal. Nucl. Chem.* **1996**, *210*, 617.
(50) Ito, Y. *Mater. Sci. Forum* **1995**, *175−178*, 627.
(51) Süvegh, K.; Klapper, M.; Domján, A.; Mullins, S.; Vértes, A. *Radiat. Phys. Chem.* **2000**, *58*, 539.
(52) Hirata, K.; Kobayashi, Y.; Ujihira, Y. *J. Chem. Soc., Faraday Trans.* **1997**, *93*, 139.
(53) Wendorff, J. H.; Fischer, E. W. *Kolloid Z. Z. Polym.* **1973**, *251*, 876.
(54) Wiegand, W.; Ruland, W. *Prog. Colloid Polym. Sci.* **1979**, *66*, 355.
(55) Götze, W.; Sjörgen, L. *Rep. Prog. Phys.* **1992**, *55*, 241.
(56) Donth, E.-J. *The Glass Transition: Relaxation Dynamics in Liquids and Disordered Materials*; Springer: Berlin, 2001.
(57) Tracht, U.; Wilhelm, M.; Heuer, A.; Feng, H.; Schmidt-Tohr, K.; Spiess, H. W. *Phys. Rev. Lett.* **1998**, *81*, 272.
(58) Bartoš, J.; Krištiac, J.; Šauša, O.; Bandžuch, P.; Zrubciva, J. *Macromol. Symp.* **2000**, *158*, 111.
(59) Bamford, D.; Reiche, A.; Dlubek, G.; Alloin, F.; Sanchez, J.-Y.; Alam, M. A. *J. Chem. Phys.* **2003**, *118*, 9420.
(60) Ngai, K. L.; Bao, L.-R.; Yee, A. F.; Soles, C. L. *Phys. Rev. Lett.* **2001**, *87*, 215901.
(61) Bartoš, J.; Krištiac, J. *J. Non-Cryst. Solids* **1998**, *235−237*, 293.

MA049067N